Design of Analog and Digital Filter of Electromyography

Latif Rozaqi
Research Centre for Electrical Power and Mechatronics
Indonesian Institute of Sciences
Bandung, Indonesia
latiefrozaqie@gmail.com

Asep Nugroho
Research Centre for Electrical Power and Mechatronics
Indonesian Institute of Sciences
Bandung, Indonesia
arthaivonita.s@gmail.com

Kadek Heri Sanjaya
Research Centre for Electrical Power and Mechatronics
Indonesian Institute of Sciences
Bandung, Indonesia
khsub79@gmail.com

Artha Ivonita Simbolon
Technical Implementation Unit for Instrumentation Development
Indonesian Institute of Sciences
Bandung, Indonesia
arthaivonita.s@gmail.com

***Abstract*—An appropriate technique of filtering is essential in dealing with bio-signal especially electromyography (EMG) because it usually contains various noises. This paper discusses the development of a low cost analog filter circuit of surface electromyography (sEMG) as well as an infinite impulse response (IIR) digital filter. An analog filter circuit with the sallen-key active filter topology is designed base on an analytical filter design and simulation. The digital IIR filter is designed simultaneously with the analog filter by deriving the IIR filter from the resulted analog filter transfer function. Furthermore, an artificial sEMG signal generated from numerical simulation as well as recorded EMG signal from Biopac MP 160 system, the standardized laboratory equipment for physiological data acquisition, is fed to the designed filter to validate the filter reliability. The result shows that the designed digital IIR filter has a better performance compared to the analog filter represented by a quantitative root mean square error (RMSE) value resulted from the two numerical simulation tests.**

Keywords—low cost, surface electromyography, analog filter, IIR digital filter

I. INTRODUCTION

The surface electromyogram (sEMG) is a popular bio-sensor used by many scientists in biomedical research. It is very simple and less invasive instrument to record human muscle activity. The resulted signal provides rich information that can be useful for many applications in the field of rehabilitation, ergonomics, sports, physiotherapy, neurophysiology, kinesiology and robotics [1]. The sEMG has several advantages compared to fine-wire or needle electrode EMG, such as easy and quick handling, less sensitive to hygiene issue, the availability of various types of disposable electrodes at low cost, and operable by researchers without professional health certification. However, the sEMG also has disadvantages in that it is only able to measure surface muscles and more prone to noise that may affect the fidelity of the EMG data. In order to acquire the required information, the signals from sEMG need to be filtered because it usually contains various noises that obscure the information. There are several dominant noise sources that are usually considered namely electrode, motion artefacts and electrical interferences. The electrode noise in sEMG usually comes from the reactive impedance due to electrode-skin contact. This impedance is very high and lead to amplitude signal reduction and waveform distortion [2]. Another source of noise is the motion artefact which can be the electrode motion on the attached cutaneous surface or cable motion artefact. The former is caused by the mechanical disturbance of electrode charge layer and the deformation of the skin under electrodes while the latter is generated from the cable as a product of unshielded cable moving through magnetic or electrical field thus generating unnecessary current. The electrode motion artefact is said to have a power density below 20Hz while the cable artefact is in the range of 1 to 50Hz [2]. The last noise source is the power line interference in which it differs in many countries but mostly is in between 50-60Hz. A filter is common to minimise the aforementioned problem. Therefore, there are many studies intended to design the filter for the sEMG application. Many references have been addressed to design analog based sEMG filter [3–8] in their research aimed to design a low cost multichannel sEMG filter with price under the available commercial sEMG filter on the market. Analogously, other research also pointed on the low cost design that are described in the two previous studies [7][9]. Another approach attempted to minimise the power consumption and reduce the size of the filter in order to fit the wearable[6]. In addition, the filter design on[4][5] was designed to detect the lower limb muscle activity.

The filter designed on the above mentioned research were said to have the frequencies of interest in between 16 Hz and 483Hz [8], 34-397Hz [6], 10-500Hz [4], 20-500Hz [3], 3-500Hz [9]. Furthermore, the complete information that sEMG's most considerable signal power is below 500Hz [2] but could be extended to 2000Hz for advanced information mining. This filter design assigns the frequency that will be observed in the range of 20 to 500 Hz that is realised by designing a bandpass filter.

II. FILTER DESIGN

Butterworth filter is chosen to be applied in this paper to deal with sEMG. The reason of choosing Butterworth filter type is because this filter has the smoothest transition in the passband through the stopband operation area, that means this filter has the least ripple compared to the other filter types namely Chebyshev, Inverse-Chebyshev and Elliptic. The filter can be designed by the following the procedure delineated on Fig. 1. It is shown the generalised process of designing any type of filter starting from the determination of filter specification followed by developing the normalised lowpass function and finally unnormalise the equation into the desired filter type.

A. Analog Filter

As the filter design procedure is clearly explained above, the first step is to determine the filter specifications. Fig. 2

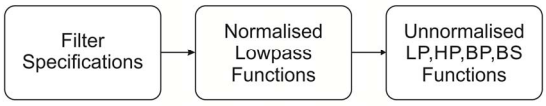

Fig. 1. Generalised Filter Design.

978-1-7281-3931-9/19/$31.00 ©2019 IEEE

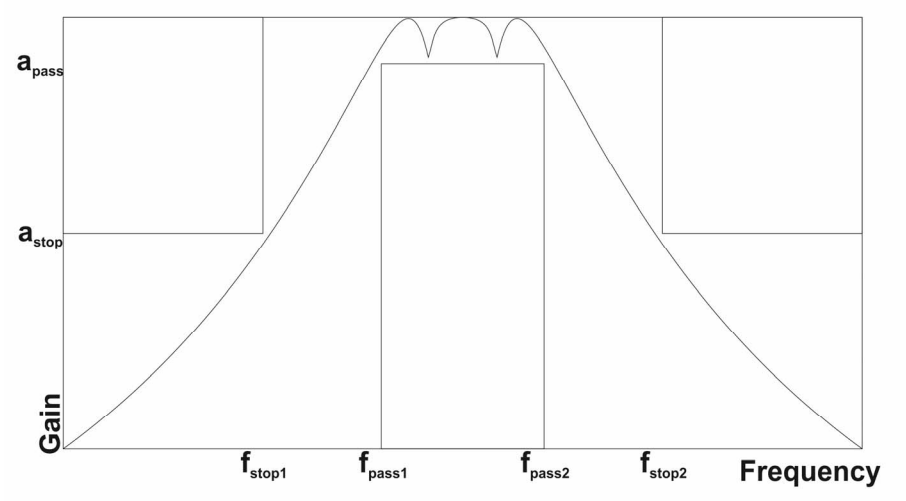

Fig. 2. Bandpass filter specification.

depicts the common parameters used to design the bandpass filter. The parameter defined is also the specification desired by the filter designer because it contains the information such as the pass and stop gain as well as the frequency of interest. The designers specify the passband a_{pass} and stopband a_{stop} gain as well as the cutoff frequencies defined as f_{pass} and f_{stop}.

As the specification is already determined. The normalised lowpass function of a Butterworth filter can further be designed by the following equation [10].

$$n_B = \frac{\log\left[\left(10^{-0.1a_{stop}}-1\right)/\left(10^{-0.1a_{pass}}-1\right)\right]}{2\log\left(\Omega_r\right)} \tag{1}$$

$$H_{B,n_B}(S) = \frac{\prod_m \left(B_{2m}\right)}{\prod_m \left(S^2 + B_{1m}S + B_{2m}\right)} \quad m = 0,1,\ldots,(n/2)-1 \quad \text{even order}$$

$$H_{B,n_B}(S) = \frac{R\prod_m \left(B_{2m}\right)}{(S+R)\prod_m \left(S^2 + B_{1m}S + B_{2m}\right)} \quad m = 0,1,\ldots,((n-1)/2)-1 \quad \text{odd order} \tag{2}$$

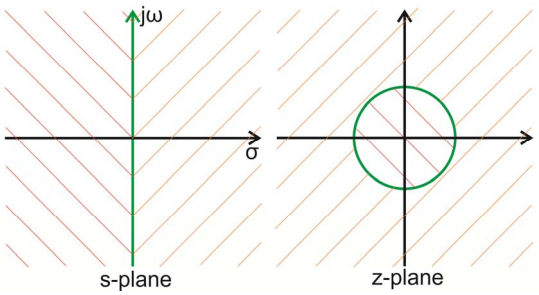

Fig. 3. z-Transform maps

where H_{B,n_B} is the normalised lowpass filter with the order of n_B while the rest of unknown variables can be determined by the equation below [10].

$$\begin{aligned} R &= \varepsilon^{-1/n} & \varepsilon &= \sqrt{10^{-0.1\cdot a_{pass}}-1} \\ B_{1m} &= -2\sigma_m & B_{2m} &= \sigma_m^2 + \omega_m^2 \\ \sigma_m &= R\cos\left(\theta_m\right) & \omega_m &= R\sin\left(\theta_m\right) \end{aligned} \tag{3}$$

After the normalised lowpass filter is determined. It can be unnormalised to any type of filter by substituting the developed equation according to the Table I. Digital Filter The IIR filter can be easily designed after the transfer function of the analog filter developed. One of the methods is z-transform. The idea is to discretise the analog transfer function that is developed from the analog filter design into a discrete transfer function. The following equation called bilinear transform can be substituted to continuous transfer function and transform continuous into discrete transfer function:

$$s = \frac{2}{T}\cdot\frac{z-1}{z+1} \tag{4}$$

This transformation that maps continuous s-domain into discrete z-domain can be seen on Fig. 3. It can be seen from the transformation that the left half part of the s-plane is mapped inside of the circle while the right half s-plane is mapped outside. Also the vertical axis is mapped on the point in the unit circle.

TABLE I. UNNORMALIZATION COEFFICIENT [10]

Type	Substitution	Coefficient
Lowpass	$S = \frac{s}{\omega_0}$	-
Highpass	$S = \frac{\omega_0}{s}$	-
Bandpass	$S = \frac{s^2+\omega_0^2}{BW\cdot s}$	$\omega_0 = \sqrt{\omega_{pass1}\cdot\omega_{pass2}}$ $BW = \omega_{pass2} - \omega_{pass1}$
Bandstop	$S = \frac{BW\cdot s}{s^2+\omega_0^2}$	$\omega_0 = \sqrt{\omega_{pass1}\cdot\omega_{pass2}}$ $BW = \omega_{pass2} - \omega_{pass1}$

TABLE II. PASSIVE COMPONENTS EQUATION[10]

Types		R	R_B/R_A	Y
Highpass		$1/\sqrt{b_2 C}$	$2-\left(b_1/\sqrt{b_2}\right)$	-
Lowpass		$1/\sqrt{b_2 C^2}$	$2-\left(b_1/\sqrt{b_2}\right)$	-
Bandstop	$a_2=b_2$	$1/\sqrt{a_2 C^2}$	$1-\sqrt{b_1^2/4b_2}$	-
	$a_2>b_2$	$1/\sqrt{a_2 C^2}$	$1+\left(b_2-a_2-b_1\sqrt{a_2}\right)/2a_2$	$R_n = \frac{2R}{[(b_2/a_2)-1]}$
	$a_2<b_2$	$1/\sqrt{a_2 C^2}$	$1+\left(a_2-b_2-b_1\sqrt{a_2}\right)/2b_2$	$C_n = \frac{C[(a_2/b_2)-1]}{2}$

III. FILTER REALISATION

A. Analog Filter

The designed analog sEMG filter block diagram is shown in Fig 4 in the red dashed rectangle in which it also shows the general analog sEMG filter that is usually consists of pre-amplification and post signal isolation stage. Here, the bandpass filter is realised by pipelining the lowpass and highpass filter. The highpass and lowpass filter cut-off is decided at 20 and 500Hz respectively.

This research aims to design the simplest and the lowest cost as well as the lowest component count as possible. Therefore, second order active filter with sallen-key topology is chosen both for highpass and lowpass filter in order to maintain the simplicity and component count while third order active bandstop sallen-key filter is used to remove the power line noise so that it can easily be realised by using quad op-amps plus single/double op-amps thus keeps the board as small as possible because only two operational amplifiers required. Because the order of the filter is already defined, therefore; the analog transfer function of the filter can be calculated using equation (1) and/or (2). Equation (5), (6), and (7) is the resulting transfer function.

$$H_{hpf,2}(s)=\frac{s^2}{s^2+247s+3.103e4} \tag{5}$$

$$H_{lpf,2}(s)=\frac{1.94e7}{s^2+6174s+1.94e7} \tag{6}$$

$$H_{bsf,3}(s)=\frac{s^6+2.487e5s^4+2.062e10s^2+5.698e14}{s^6+401.3s^5+3.292e5s^4+7.462e7s^3+2.730e10s^2+2.758e12s+5.698e14} \tag{7}$$

Note that the center bandstop filter frequency is chosen to be 50Hz as mains frequency on this country lies on 50Hz. The sallen-key active filter topology and its form is shown on Fig. 5.

Equation (8), (9), and (10) the general form that holds the filter transfer function of the Fig. 5.

$$H_{hpf,odd}(s)=\frac{s}{s+b_2} \qquad H_{hpf,even}(s)=\frac{s^2}{s^2+b_1 s+b_2} \tag{8}$$

$$H_{lpf,odd}(s)=\frac{a_2}{s+b_2} \qquad H_{lpf,even}(s)=\frac{a_2}{s^2+b_1 s+b_2} \tag{9}$$

$$H_{bsf,odd/even}(s)=\frac{\left(s^2+a_2\right)}{s^2+b_1 s+b_2} \tag{10}$$

The passive components values can be obtained directly by substituting the constants in equation (8)-(10) into Table II.

B. Digital Filter

The IIR digital filter is realised by discetise the developed analog transfer function in equation (8)-(10). The three stage filter shown in Fig. 6 can be combined to form single transfer function that represents the overall sEMG filter designed.

The resulting analog sEMG filter is (11).

$$H_{EMG}(s)=\frac{1.94e7s^8+4.824e12s^6+3.999e17s^4+1.105e22s^2}{s^{10}+6822s^9+2.386e7s^8+1.558e10s^7+1.001e13s^6+3.623e15s^5+1.16e18s^4+2.423e20s^3+4.211e22s^2+4.499e24s+3.43e26} \tag{11}$$

The developed sEMG analog filter transfer function is then transformed to discrete transfer function by substitute equation (4) into equation (11) and produce the following result. Note that the sampling time is chosen to be $T=0.001s$.

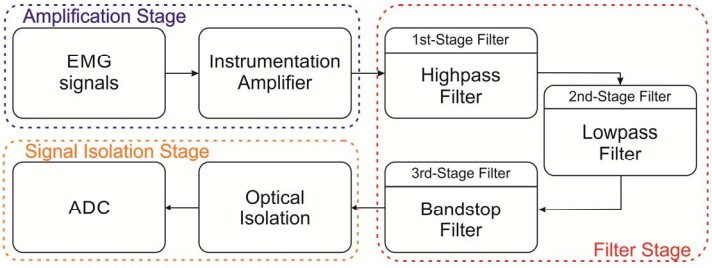

Fig. 4. Block diagram of designed analog circuit.

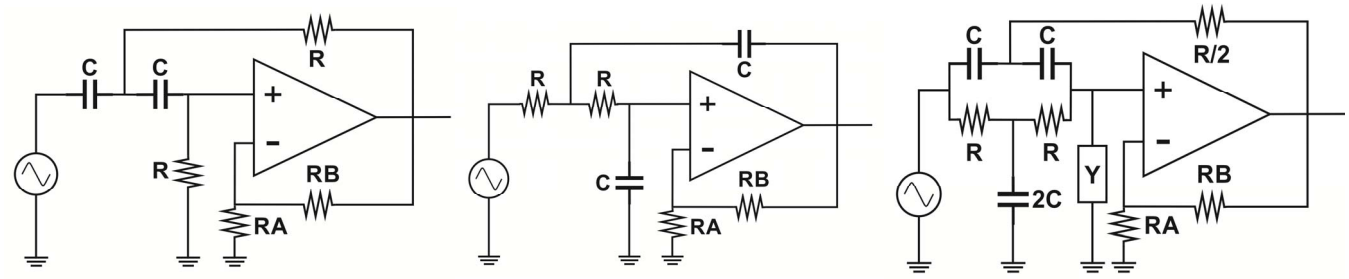

(a) (b) (c)

Fig. 5. Sallen-key active filters topology (a) Second order Highpass filter (b) Second order Lowpass filter and (c) First order Bandpass filter

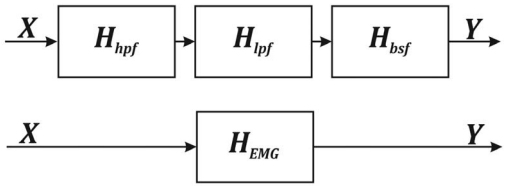

Fig. 6. Block diagram combination

$$H_{EMG}(z)=\frac{0.3942z^{10}-2.269z^{9}+4.748z^{8}-2.785z^{7}-5.142z^{6}+10.11z^{5}-5.142z^{4}-2.785z^{3}+4.748z^{2}-2.269z+0.3942}{z^{10}-6.274z^{9}+16.66z^{8}-23.78z^{7}+18.72z^{6}-7.055z^{5}+0.8158z^{4}-1.123z^{3}+1.776z^{2}-0.912z+0.1632} \quad (12)$$

IV. Results and Discussion

Passive components chosen to build the analog filter circuit of sEMG is shown in Table III. A 0.1uF capacitor is selected for highpass and lowpass filter while the notch filter capacitor is 0.01uF. After conducting numerical simulation, the frequency response resulted from the the theoretical analog filter designed is illustrated in Fig. 7. The frequency response from the analog filter through spice simulation after decide and adjustment process of passive component selection used on the circuit is also shown on the same figure. Both of the designed analog and digital filter is then verified by comparing the signal generated from the simulation as well as from a signal recorded from Biopac. Therefore, simulated sEMG data has been generated from the following equation [11]. Equation (13) can generate the artificial sEMG signal based on the probability density function by determining two sets of constantans. (μ,λ) The signal result is depicted in Fig. 8.

$$f(x;\mu,\lambda)=(\lambda/2\pi)^{\frac{1}{2}}x^{-\frac{2}{3}}\exp\left(-\lambda(x-\mu)^2/2\mu^2x\right),\ x>0;\quad \mu>0;\quad \lambda>0; \quad (13)$$

where: μ is the mean, λ is the shape parameter.

In order to simulate the noise, an artificial power line noise is added to the ideal signal of sEMG. The power line noise contains a centered frequency of 50Hz. Fig. 9 shows the sEMG filter that is colored by power line noise. The noised sEMG is then carried out as a source signal that is passed to the designed analog and digital filter. At the first glance, the designed analog and digital filter can effectively remove the power line noise as it can be seen in Fig. 10. It is further strengthened by the fact from the comparison of frequency domain analysis which is shown on Fig. 11. Furthermore, the root mean square error (RMSE) is defined as a quantitative analysis tool to examine the filter effectivity. Equation (14) holds the RMSE equation.

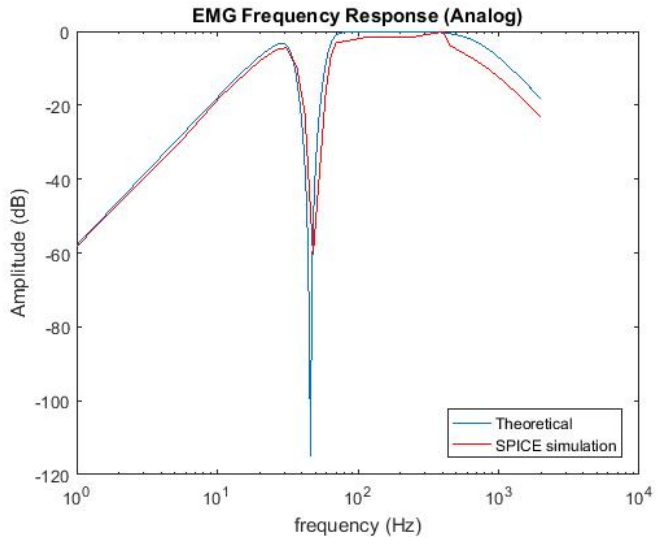

Fig. 7. Analog filter frequency response

$$RMSE=\sqrt{\frac{1}{N}\sum_{n=1}^{N}(\hat{x}[n]-x[n])^2} \quad (14)$$

where N is the number of samples, $\hat{x}[n]$ is the reference signal, $x[n]$ is the filtered sEMG signal.

The result of the RMSE calculation resulted from applying equation (14) is shown on Table IV, note that $\hat{x}[n]$ is chosen to be the simulated clean sEMG signal. Further examination is performed by giving the raw data recorded from sEMG using a Biopac MP 160 physiological data acquisition system to be applied to the filters. At this stage,

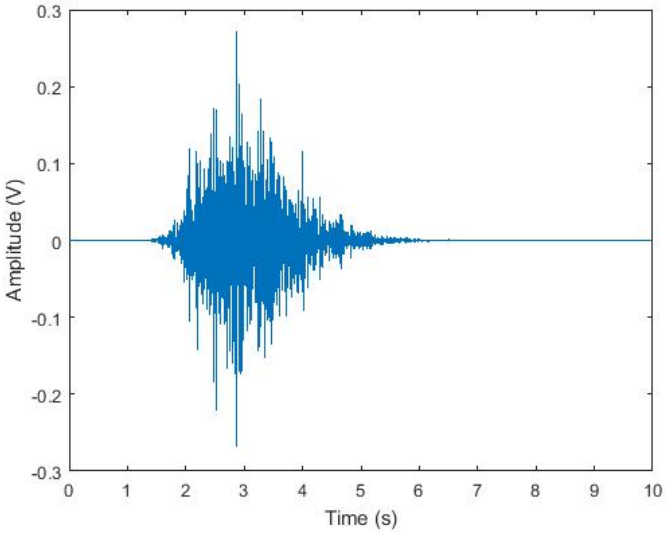

Fig. 8. Simulated clean sEMG signal

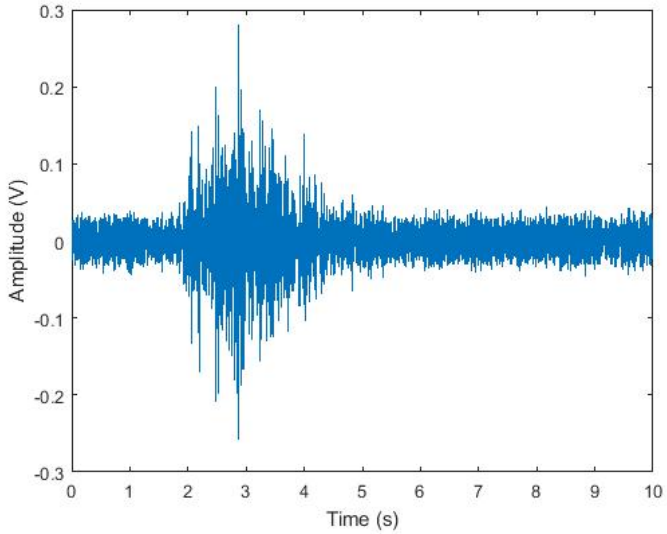

Fig. 9. Simulated sEMG with the addition of power line noise

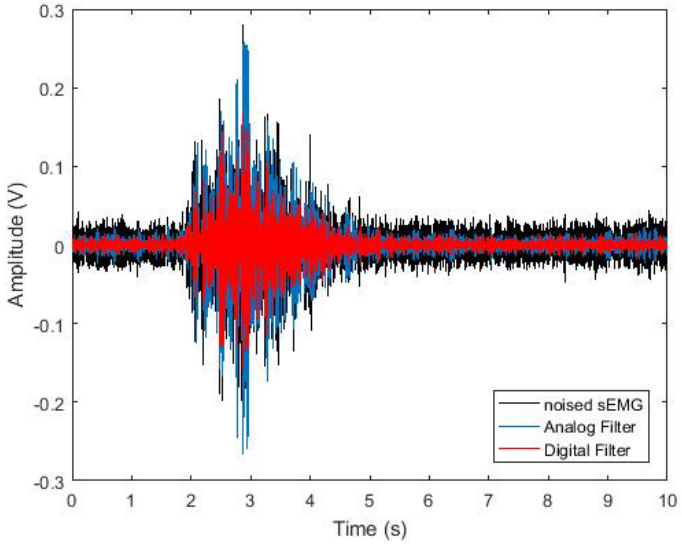

Fig. 10. Simulated sEMG signal comparation on time domain

signals are acquired from a free arm movement in which sEMG electrodes record the biceps and triceps brachii muscles activity. The raw signal generated from the aforementioned muscle activity as well as the filtered signal of developed analog, digital IIR and the Biopac system is shown in Fig. 12. Furthermore, Fig. 13 shows the zoomed view of recorded sEMG from the Biopac system that is highlighted by the red-dashed rectangle in Fig. 12. The filter efficacy can be quantized by applying the same formula of equation. (14) that results in Table V and by changing the reference signal $\hat{x}[n]$ to be the result of the Biopac system filter signal.

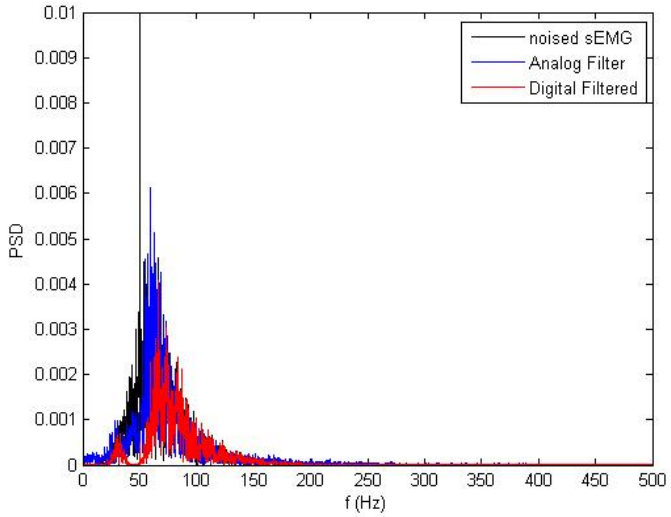

Fig. 11. Simulated sEMG signal comparison in frequency domain

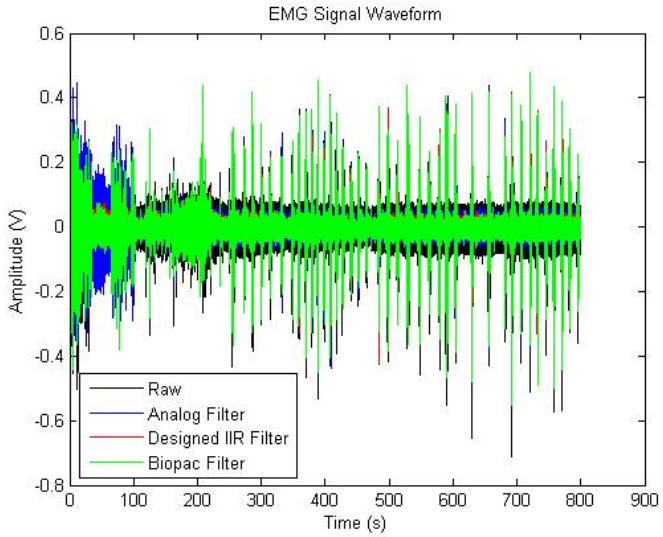

Fig. 12. Overall view of sEMG signal recorded from Biopac MP160

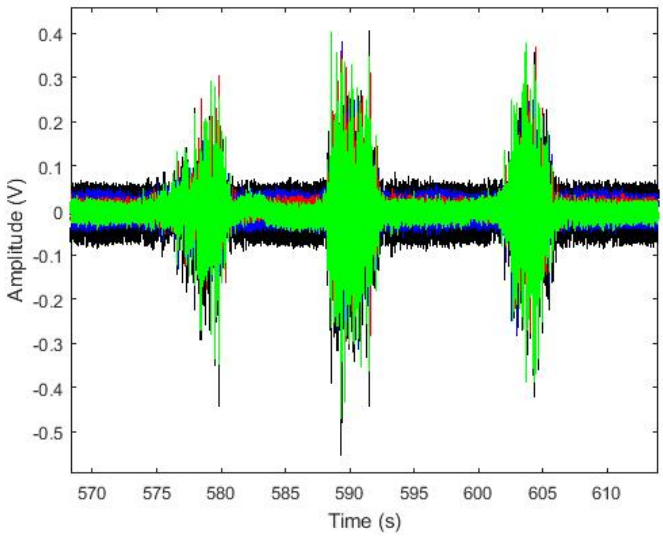

Fig. 13. Zoomed view of sEMG signal

TABLE III. SELECTED PASSIVE COMPONENTS

No	R_n	RA	RB	Y
Highpass				
1	56kΩ	10kΩ	6.2kΩ	-
Lowpass				
1	2.7kΩ	10kΩ	6.2kΩ	-
Bandstop				
1	330kΩ	10kΩ	6.2kΩ	-
2	330kΩ	10kΩ	12kΩ	R_0 =880kΩ
3	330kΩ	10kΩ	12kΩ	C_0 =5nF

TABLE IV. RESULTED FILTER RMSE VALUE

No	Filter	RMSE
1	Analog	0.06113
2	Digital IIR	0.03613

TABLE V. RESULTED FILTER RMSE VALUE

No	Filter	RMSE
1	Analog	0.05665
2	Digital IIR	0.05224

V. CONCLUSION

Analog and digital sEMG filter have been designed. Both of the designed filter was given an appropriate test through the numerical simulation. An artificial sEMG signal as well as recorded muscles activity signals using the Biopac system is fed to the designed filter and a quantitative analysis using the root mean square error (RMSE) was performed to compare both of the developed filter. Both of the test results indicate that digital filter was able to outperform the analog filter. The test from feeding an artificial sEMG signal shown the RMSE of the analog filter is higher than the digital one, the analog filter RMSE was 0.06113 while the digital is 0.03613. Furthermore, the test utilising the recorded Biopac system signal exhibit the same pattern in which the analog and digital filter have the RMSE of 0.05665 and 0.05224 respectively. It is clear that the digital filter can outperform the analog filter because the analog filter accuracy suffers from the decide and adjustment process on choosing the passive components value such as the existence of components, tolerance, manufacturing imperfection, performance degradation etc.

ACKNOWLEDGMENT

The authors gratefully acknowledge the support from the ministry of research, technology and higher education of republic Indonesia for the funding of this study through INSINAS research funding scheme with the contract number 15/INS-1/PPK/E4/2019.

REFERENCES

[1] R. Merletti, A. Botter, A. Troiano, E. Merlo, and M. A. Minetto, "Technology and instrumentation for detection and conditioning of the surface electromyographic signal: State of the art," *Clin. Biomech.*, vol. 24, no. 2, pp. 122–134, Feb. 2009.

[2] E. . Clancy, E. . Morin, and R. Merletti, "Sampling, noise-reduction and amplitude estimation issues in surface electromyography," *J. Electromyogr. Kinesiol.*, vol. 12, no. 1, pp. 1–16, Feb. 2002.

[3] J. Wang, L. Tang, and J. E Bronlund, "Surface EMG Signal Amplification and Filtering," *Int. J. Comput. Appl.*, vol. 82, no. 1, pp. 15–22, Nov. 2013.

[4] M. S. Al-Quraishi, A. J. Ishak, S. A. Ahmad, and M. K. Hasan, "Multichannel EMG data acquisition system: Design and temporal analysis during human ankle joint movements," in *2014 IEEE Conference on Biomedical Engineering and Sciences (IECBES)*, 2014, no. December, pp. 338–342.

[5] H. M. Desa, M. S. Zuber, R. Jailani, and N. M. Tahir, "Development of EMG circuit for detection of leg movement," in *2016 IEEE Symposium on Computer Applications & Industrial Electronics (ISCAIE)*, 2016, pp. 46–51.

[6] D. A. F. Guzman, S. Sapienza, B. Sereni, and P. M. Ros, "Very low power event-based surface EMG acquisition system with off-the-shelf components," in *2017 IEEE Biomedical Circuits and Systems Conference (BioCAS)*, 2017, vol. 2018-Janua, pp. 1–4.

[7] N. Mohammed, Z. Ahmed, and R. Alam, "Design and development of low-cost EMG amplifier for assistive technology," in *2017 IEEE International Conference on Power, Control, Signals and Instrumentation Engineering (ICPCSI)*, 2017, pp. 137–140.

[8] I. A. R. da Silva, E. C. B. F. dos Santos, E. M. Carvalho, and D. O. Dantas, "Low cost hardware and software platform for multichannel surface electromyography," in *2018 IEEE Symposium on Computers and Communications (ISCC)*, 2018, vol. 2018-June, pp. 01114–01119.

[9] T. Supuk, A. Skelin, and M. Cic, "Design, Development and Testing of a Low-Cost sEMG System and Its Use in Recording Muscle Activity in Human Gait," *Sensors*, vol. 14, no. 5, pp. 8235–8258, May 2014.

[10] L. Thede, "Practical Analog and Digital Filter Design, Artech House," *Inc., Norwood*, vol. 3, no. 5, pp. 187–188, 2004.

[11] I. Ashida, S. Kawakami, and Y. Miyaoka, "A new method of simulating surface electromyograms using probability density functions," *Comput. Biol. Med.*, vol. 38, no. 7, pp. 837–844, Jul. 2008.